

A Millimeter-wave Phased Array Radar for Hazard Detection and Avoidance on Planetary Landers

Brian D. Pollard, Gregory Sadowy, Delwyn Moller, and Ernesto Rodríguez
Jet Propulsion Laboratory
California Institute of Technology
4800 Oak Grove Drive
Pasadena, CA 91109
818.354.7718
pollard@jpl.nasa.gov

Abstract— Safe, precise landing in difficult planetary terrain, including areas that are rocky, heavily sloped, or both, requires remote sensing of the surface in order to choose an appropriate landing site. While active or passive optical sensors might seem appropriate for this application, we are developing an alternate approach based on a millimeter-wave electrically scanned phased array radar. A radar offers several advantages over present optical sensors, including a substantial reduction in dust or engine plume susceptibility, a larger range of operating altitudes, and a coherent measurement of the platform velocity.

In this paper, we describe the overall system design for a radar being developed for the NASA Mars Science Laboratory, set to launch in 2009. We discuss the terminal descent scenario, and the requirements imposed by the terminal guidance and landing vehicle hazard tolerance. We present the digital elevation and roughness map generation performance of our candidate sensor as derived from terminal descent simulations over synthetic Mars terrain, where roughness is derived from a optimal threshold crossing algorithm. We also present a novel, fast velocity vector retrieval algorithm that avoids the necessity of inverting the entire phase matrix, making it ideal for onboard computation.

Finally, we describe our upcoming hardware development efforts, including the development of a system test bed that will be used in the prototype sensor. This system is capable of the required 1 GHz bandwidth and five hops in center frequency. Our future development and testing plans will use this test bed to develop a full millimeter-wave phased array, leading to a unique hazard detection sensor for this exciting mission.

TABLE OF CONTENTS

1. INTRODUCTION	1
2. TERMINAL DESCENT SCENARIO	1
3. SYSTEM REQUIREMENTS	2
4. BASIC SYSTEM ARCHITECTURE	3
REFERENCES	8

¹0-7803-7231-X/01/\$10.00/© 2002 IEEE

¹ IEEEAC PAPER #1188, UPDATED OCT 14, 2002

1. INTRODUCTION

Past lunar and martian landing missions have actively sensed the landing surface during the terminal descent phase, but have uniformly done so with respect to obtaining altitude and / or velocity information. Nearly all recent landing missions, including the Mars Viking Mission (1976), Mars Pathfinder (1997), Mars Polar Lander (1999), and the upcoming twin Mars Exploration Rover (set to launch in 2003) made use of radar altimetry; Viking and Mars Polar Lander were further distinguished by the use of radar for sensing of the lander velocity vector.

While sensing of the lander altitude and velocity are necessary portions of a descent and landing system, safe landing in difficult terrain may also require imaging of the landing surface and detection of hazards. The upcoming Mars Science Laboratory (MSL) mission, set to launch in 2009, is currently expected to include such an imaging sensor as a part of an active hazard avoidance system. Proposed imagers for that system include active and passive optical systems, and the alternative described in this paper, an active millimeter wave phsaed array radar.

In the following sections we describe a nominal terminal descent scenario for the MSL mission, and discuss the appropriate requirements imposed by the terminal guidance and landing vehicle. We then present a basic radar system architecture designed to meet those requirements, and describe the necessary algorithms and available products, including the sensor altitude, digital terrain maps of the landing surface, digital roughness maps of the landing surface, and the spacecraft velocity vector.

We conclude with a discussion of the key technologies required for sensor development, and discuss present and planned hardware prototype and system verification efforts.

2. TERMINAL DESCENT SCENARIO

The basic terminal descent scenario is discussed fully in [1] (and the references therein), and summarized in Figure 1. We briefly summarize the scenario here in order to establish context for the radar, and to motivate the requirements discussion below.

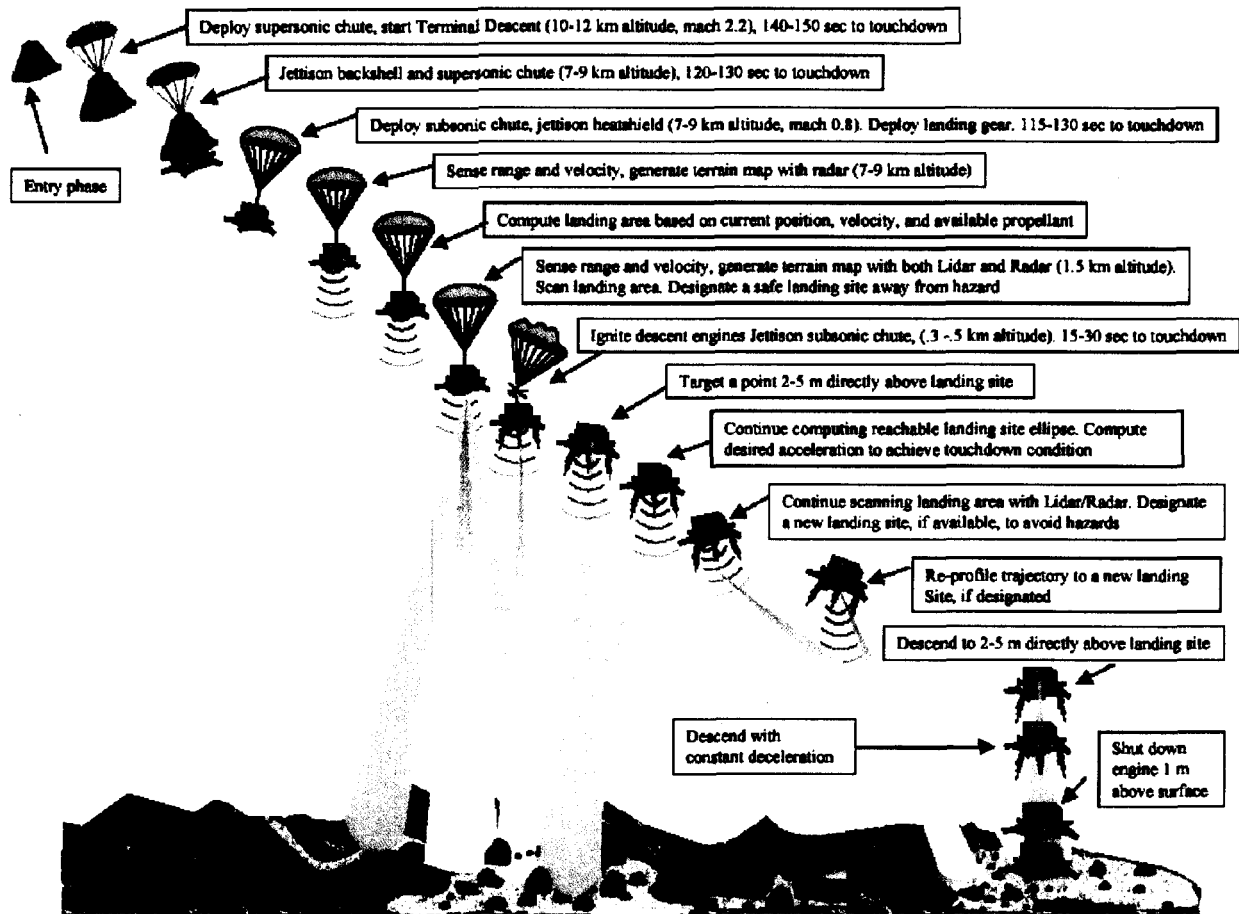


Figure 1: Terminal descent scenario, as shown in [1].

The entry phase consists of initial entry into the Martian atmosphere, and, once the vehicle has slowed and reached an altitude of 10-12 km above the surface, the deployment of a supersonic parachute. Throughout this phase, the entire lander is encased in a heat shield and backshell, protecting against aerodynamic loads and heating, and prohibiting any terrain sensing.

After the vehicle has slowed to an appropriate velocity (at an altitude of some 7-9 km), the backshell and supersonic parachute are jettisoned, a subsonic parachute is deployed, and the heatshield is jettisoned. At this point, the radar commences operation.

The lander remains on the subsonic parachute until an altitude of 300 to 500 m, at which time the chute is jettisoned, descent engines are ignited, and a safe landing site is chosen. At this point, there are approximately 15 to 30 seconds left until touchdown. The amount of propellant available can allow for a maximum 100 m horizontal divert from the 500 m altitude.

Under the power of the descent engines, the lander maneuvers to a point 2 to 5 m above the chosen landing site. At this point, the horizontal velocity must be nulled to less than 1 m/s. The lander then descends with constant

deceleration to an altitude of 1 m, at which time the engines are turned off, and the lander drops to the surface.

Based on the present design of the landing pallet (see the discussion in [J]), a safe landing site is defined as one with hazards (rocks) smaller than 1 m in vertical extent, and with slopes over several meters less than 30° . This, and the other altitude and velocity requirements, drive the sensor requirements and design as described in the next section.

3. SYSTEM REQUIREMENTS

Based on the descent scenario described above, a preliminary set of system requirements on a joint velocity-altitude and imaging radar sensor can be derived. The values discussed in this section are summarized in Table 1.

Altitude Range of Operation

As we discuss in Section 2, the earliest opportunity for the radar to sense the terrain is after the heatshield is jettisoned, shortly after the deployment of the subsonic parachute. The altitude of this transition is on the order of 7-9 km, and can be considered the maximum required altitude of operation.

The minimum altitude of operation is determined by the altitude at which the engines are turned off, nominally 1 m above the surface.

Altitude and Elevation Map Accuracy and Precision

As the lander enters its final maneuver (beginning at 5 m), the altitude sensing accuracy and precision can also be determined from the engine turn off level of 1 m. If a 10% error can be accommodated by the landing system, we arrive at a 10 cm total error requirement. If the absolute accuracy and precision components are equally divided, we can set a low altitude height accuracy of 7.1 cm, and a similar value for the altitude precision.

At higher altitudes, the absolute accuracy is less of an issue; we have chosen 1 m as a preliminary value. More of an issue is the ability to estimate or remove a slope from a terrain map. If we are interested in sensing slopes of 30° or greater to within 10% from an altitude of 500 m, we can estimate, given 5 m pixels (see Section 5), that a precision of 20 cm is required.

Velocity Component Accuracy and Precision

At the time of final descent (5 m), the velocity must be nulled to less than 1 m/s. Assuming a 10% tolerance on that value, the total velocity accuracy and precision must be on the order 10 cm/s. As above we split this allocation equally between accuracy and precision.

At higher altitudes, based on preliminary discussions (D.Burkhart, personal communication), a value of 20 cm/s is set.

System Field of View

Based on a 100 m maximum divert at an altitude of 500 m, we can set a required field of view of +/- 11.3°. Note that the motion of the spacecraft on the parachute may place more stringent requirements on the maximum view angle, but this requirement has not yet been determined.

Hazard Detection and Avoidance

As discussed in Section 2 (and in [2]), the lander can safely touchdown on hazards of 1 m, and slopes of 30°. These hazards and slopes must be detectable to a high (99%) probability at an altitude of 500 m. These two requirements drive the radar design to achieve a high pixel resolution, as discussed in the following two sections.

Table 1: Basic system requirements on a altitude, velocity, and hazard detection radar, based on a nominal MSL terminal descent scenario.

Parameter	Units	Value
Maximum Altitude of Operation	m	9000
Minimum Altitude of Operation	m	1
DEM Accuracy – below 5 m	cm	7.1
DEM Precision – below 5 m	cm	7.1
DEM Accuracy – above 5 m	cm	100
DEM Precision – above 5 m	cm	20
Velocity Accuracy – below 5 m	cm/s	7.1
Velocity Precision – below 5 m	cm/s	7.1
Velocity Accuracy – above 5 m	cm/s	14.1
Velocity Precision – above 5 m	cm/s	14.1
Field of View	deg	11.3
Minimum Hazard to Detect at 500 m	cm	100
Minimum Slope to Detect at 500 m	deg	30

4. BASIC SYSTEM ARCHITECTURE

The need for high pixel resolution would typically lead one to a synthetic aperture radar design. In this situation, however, the descent profile is quite unpredictable, and horizontal motion during critical stages of the descent is not assured. In addition, the real time motion knowledge and processing requirements could be quite severe. These two factors have lead us to reject such an approach.

In other space or airborne cases, a side-looking real aperture can eliminate the dependence of range resolution on antenna size through the use of range compression. Again, in this situation, the requirement of a 0 to +/-11 degree field of view makes such an approach difficult to implement.

With the above to approaches eliminated, we can say that the basic radar architecture to meet the system requirements have a pixel size dependent primarily on the effective antenna size of the radar, and a vertical resolution dependent primarily on the system bandwidth. Those factors, coupled with the need for a high frame rate, have lead us to choose a high frequency real aperture phased array radar architecture.

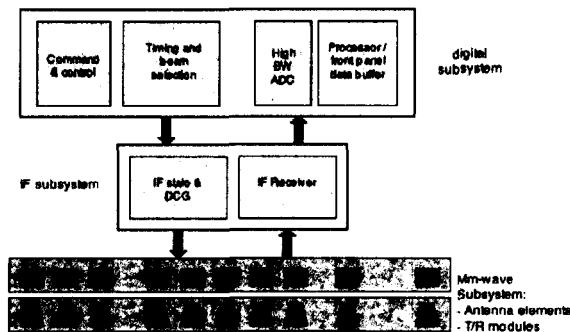


Figure 2: System block diagram, including the digital, intermediate frequency (IF), and millimeter-wave subsystems.

The basic system architecture is shown in Figure 1. Each beam is selected digitally through the control of the system phase shifters, and the pulse is generated at the intermediate frequency (IF). Following generation, each pulse is modulated by a chirped waveform and passed to the antenna array. Each element within the array contains a transmit/receive (T/R) module mouted directly to the radiating element or aperture. The upconversion to the millimeter-wave center frequency would take place at the T/R module.

Upon reception, each signal is downconverted at the T/R module, passed to the IF receiver, downconverted to video frequencies, and digitized by a high-bandwidth analog-to-digital converter (ADC). The received data from each beam is then range compressed and detected in an onboard data processor, which also estimates initial data products.

Several additional radar features are expected, based on the system requirements. These include multiple “hops” in center frequency to increase the number of independent samples, multiple pulses transmitted on each beam to allow for coherent velocity detection, and thinning of the antenna aperture to allow for reductions in mass. These factors are discussed further in Section 6. First, however, we discuss in additional depth the available data products and algorithms necessary to produce those products.

5. SYSTEM DATA PRODUCTS AND ALGORITHMS

Three basic data products are necessary from this radar: mean elevation of a given pixel, the roughness or hazard properties of a pixel, and the velocity vector. These three products are discussed in this section.

Pixel Mean Elevation

The elements necessary to estimate elevation and altitude from a returned radar power waveform include knowledge of the radar position, direction that the radar antenna beam is

pointed, and time of flight of the returned signal. The first parameter is known by the lander terminal guidance, and the second is known through radar control software (to within the accuracy of the antenna pointing) ; the remaining parameter is the range to the surface. As the system timing and analog delay through the system can be well known, the only algorithm requirement is the determination of the mean elevation from the returned waveform.

Elachi et al. [3] address the multiple methods of determining the mean elevation given a returned power waveform, including peak finding, threshold crossing, half energy, and centroid estimation. The centroid estimation method, illustrated on a sample waveform in Figure 2, is consistently the most accurate method, particularly for low numbers of independent samples, or “looks”.

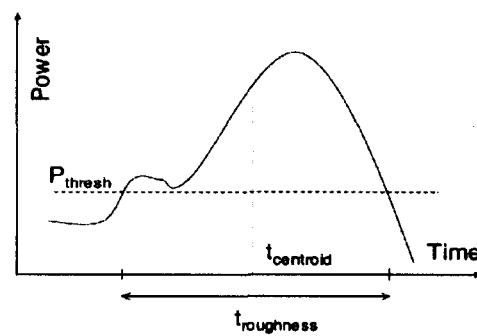


Figure 3: Cartoon of the returned power waveform from a given beam or pixel. Shown are the time (or range) centroid used to derive the mean elevation, and the temporal return width ($t_{\text{roughness}}$), used to derive the pixel roughness.

Pixel Roughness

The high requirements on detection probability and the real-time need for the data directly impact the pixel roughness algorithm: it must be robust and it must be computationally efficient. Robustness dictates that minimal assumptions be made about the returned waveform, and computational efficiency also limits the possibility of using sophisticated fitting. We also note that the number of looks may be limited, given the nadir looking geometry and possible lack of horizontal motion.

Our minimal set of assumptions include that fact that the number of looks and the speckle and thermal noise characteristics of the instrument are known a priori, and that a hazard must have a width to height ratio limited to a realistic range. This latter fact allows us to assume that hazards of a given height must occupy a minimum area within the resolution cell, and thus have a minimum signal to clutter ratio relative to the return from the rest of the pixel.

In order to detect a hazard, we use the fact that, in the presence of within-pixel topography, the length of the radar return duration will be increased by an amount proportional

to the hazard height or pixel slope. The return pulse duration is determined by a simple threshold-crossing algorithm illustrated in Figure 2, and a comparison against the expected pulse duration yields a probability of hazard detection.

The primary challenge in this process is the avoidance of false alarms. We accomplish this by proceeding hierarchically: an initial search is made for the largest feasible hazard, given the pixel size. This process is illustrated in Figure 3. The detection thresholds are selected by assuming a minimum signal to clutter ratio for this size and selecting the threshold crossing values and the maximum range separation from the pixel center to maximize the probably of detection and minimize the probability of false alarm. If no detection occurs, the range extent to be examined is reduced, and new thresholds are selected based on the changed signal to clutter ratio. The procedure ends when the maximum hazard size drops below an acceptable value. After the algorithm has terminated for that pixel, a probability of detection is assigned to that pixel. This probability is refined using subsequent pulses and a final determination of the presence of a hazard is made based on the multi-pulse detection probability.



Figure 4: Flow diagram of the roughness algorithm, which steps through multiple expected hazard or slope sizes in order to set the optimal threshold and search area.

Velocity Vector

The velocity vector is derived from coherent measurements of the line of sight velocity measured on each beam. In general, given a circular coordinate system and a beam pointed at an angle of θ and ϕ , the measured velocity is

$$v_m(\theta, \phi) = v_x x(\theta, \phi) + v_y y(\theta, \phi) + v_z z(\theta, \phi) \quad (1)$$

where x , y , and z are the typical projections of θ and ϕ into rectangular coordinates,

$$\begin{aligned} x(\theta, \phi) &= \sin(\theta) \cos(\phi) \\ y(\theta, \phi) &= \sin(\theta) \sin(\phi) \\ z(\theta, \phi) &= \cos(\theta). \end{aligned} \quad (2)$$

Given a set of beams, we can construct a set of equations for each measurement such that

$$\mathbf{M} = \mathbf{P} * \mathbf{V} \quad (3)$$

where \mathbf{M} is a vector containing the measured velocities, \mathbf{P} is a matrix of the x , y , and z projections for each beam, and \mathbf{V} is the three-dimensional velocity vector. To obtain \mathbf{V} given the measurements \mathbf{M} , we must simply invert (3). In practice, however, such matrix inversion can be time consuming, a critical point given the real-time need for the data. For this application, however, there is a simple method, discussed in Appendix A, for obtaining the velocity vector from a simple slope calculation on an image of measured velocities.

In order to measure the line of sight velocity, a simple "pulse-pair" phase estimation approach is adopted [4] to estimate the first moment of the received Doppler spectrum. Given a pulse transmitted at time t_1 , with a range to the surface along the boresight vector of r_1 , and a second pulse transmitted at $t_2 (= t_1 + \Delta t)$, with a range of r_2 , the argument of the correlation product, q , is

$$q = \arg(v_1 v_2^*) = k(r_1 - r_2) \quad (4)$$

where v_1 and v_2 are the received signals at t_1 and t_2 , respectively, and k is the electromagnetic wavenumber. The mean velocity is then

$$v' = -(q \lambda / 4\pi \Delta t) \quad (5)$$

The error in estimating the line of sight velocity can be calculated as [5]

$$\sigma_v = \frac{\lambda}{2} \frac{\sqrt{\rho^{-2}(\Delta t)(1 + \text{SNR}^{-1}) - 1}}{\sqrt{2N} 2\pi \Delta t} \quad (6)$$

where N is the number of looks, SNR is the signal-to-noise ratio, and $\rho(\Delta t)$ is the target correlation coefficient.

6. SYSTEM DESIGN AND PERFORMANCE

Based on the algorithm descriptions above, we can now derive a set of more detailed system parameters based on meeting the requirements of Table 1.

Number of Available Looks

As briefly mentioned in the text above, the number of looks available, given the nadir looking geometry and the uncertainty in the horizontal velocity profile, is not known. Given that additional looks from horizontal motion cannot be guaranteed, we have chosen to include a frequency "hopping" capability in the basic radar design. This capability uses up to 5 changes in center frequency to generate independent looks, and we use that number as a

lower bound throughout the performance analysis that follows.

Mean Pixel Topography

The sub-10cm requirements on mean pixel topography precision and accuracy drive us to as fine a sampling frequency and system bandwidth as possible: the resolution in range is necessary to determine the centroid with this type of accuracy. Based on the availability of high speed ADCs, we have chosen a 1 GHz system bandwidth (15 cm vertical resolution), and a corresponding 1 Gs/s sampling system.

We have evaluated the performance of the centroid algorithm with a simple, coherent point target simulation of moderately sloped (0° to 30°) terrain. Given a SNR greater than 10 dB, the above mentioned system bandwidth, and 5 looks, the system is capable of 5 to 7 cm precision in mean topography estimation (for scan angles out to 12°).

The mean topography accuracy is dependent upon several factors, including the stability of the system group delay and timing jitter. Based on experience with standard nadir altimeters (including Topex/Poseidon), a 7 cm accuracy over the short flight time of this radar should be achievable.

Velocity Vector

Based on (6), the velocity component precision can be evaluated, given the SNR, the number of looks, and the pulse-pair separation time. The optimal pulsing scheme would allow for as long a pulse-pair separation time as is possible while maintaining a coherent target, and maintaining the required fast scan time. As a preliminary number, we use a Δt of 40 μ s. Given such a value, and 94 GHz center frequency, and an SNR of 10 dB, a value of 60 cm/s is achievable on a per-pixel basis. However, the actual radial velocities are averaged by the velocity conversion algorithm described in Appendix A. When applied to that algorithm, the resulting a horizontal component velocity precision of better than 4 cm/s. The vertical velocity can also be extracted from that algorithm, yielding a component precision of approximately 8 cm/s.

At lower altitudes, when the SNR approaches a high value, the velocity precision should be well below the 7.1 cm/s requirement.

Hazard Detection

The performance of the hazard detection algorithm is highly dependent on the number of looks, which we have fixed at 5, and the pixel resolution, or, given the 500 m detection algorithm requirement, the system beamwidth. The maximum scan angle of 11.3° is also a limiting factor.

We can take a preliminary view of the relationship between maximum detectable hazard, scan angle, and beamwidth by viewing the width of a returned pulse (as measured by the 10 dB points in the range profile). Figure 4 shows this relationship. The x-axis has antenna size for a 94 GHz

antenna, while the y-axis shows the scan angle. The color image then shows the ground-projected distance of the 10 dB antenna beamwidth, or, equivalently, the roughness for a threshold set 10 dB below the peak (see Figure 2).

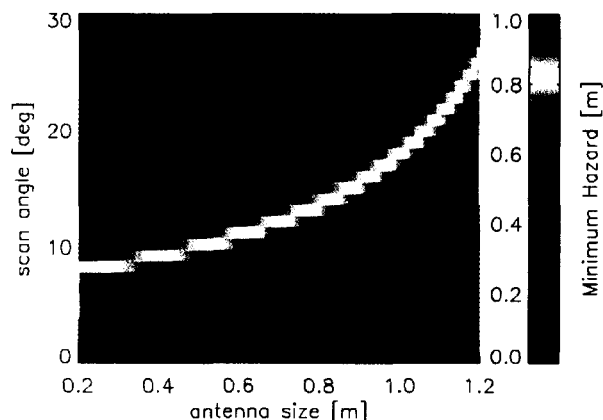


Figure 5: Maximum detectable hazard (10 dB beamwidth) as a function of antenna size (beamwidth) versus scan angle.

For a scan angle of 11.3° , a 1 m “hazard” requires an antenna size of ~ 0.5 m, or a beamwidth of 6.4 mrad. A similar beamwidth at 35 GHz would require a 1.4 m antenna.

Given a slightly smaller antenna size (7.7 mrad), we have tested the hazard detection algorithm described in the previous section using a point target simulation of hazards on flat terrain. A sample waveform is shown in Figure 5. Based on the results of this simulation and the previously discussed system parameters (>10 dB SNR, 1 GHz bandwidth, and 5 looks), we find that we can detect 1 m hazards from 500 m with a probability approaching 95%. An additional independent 5 frequency image of the target can raise this detection probability to above the required 99%.

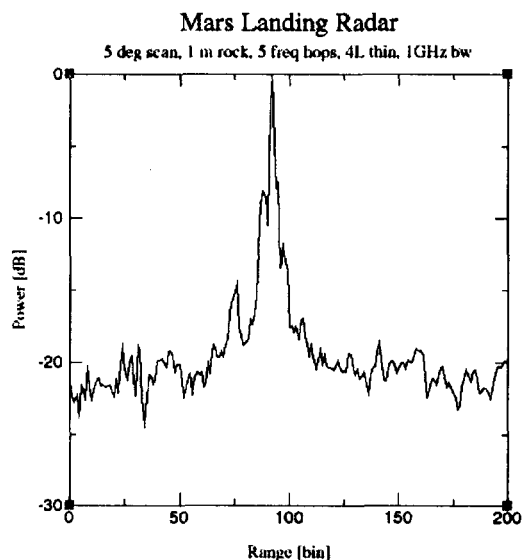


Figure 6: Sample point-target simulation waveform of a 1 m hazard on flat terrain at a scan angle of 5 degrees. The hazard is clearly visible to the left of the ground return.

System Summary

Based on the above assumptions, we can construct a key set of system parameters. Table 2 shows a set for a 94 GHz center frequency design, while Table 3 shows a set for a 35 GHz center frequency design.

Table 2: Key radar parameters for a 94 GHz design.

Parameter	Units	Value
Center frequency	GHz	94.0
Wavelength	mm	3.19
Antenna Size	m ²	0.5 x 0.5
Element Beamwidth	deg	15.2
Array Beamwidth	mrاد	7.7
Power per Element	dBm	10.0
Number of Elements	-	128
Total Transmit Power	dBm	31.1
Element Noise Figure	dB	8.0
System Noise Bandwidth	GHz	1.0
Number of Frequency Hops	-	5
Pulsewidth	μs	1.0 – 10.0
Noise Equivalent σ ₀ (9000m)	dB	-22.5
Noise Equivalent σ ₀ (500m)	dB	-27.6

Table 3: Key radar parameters for a 35 GHz design.

Parameter	Units	Value
Center frequency	GHz	35.0
Wavelength	mm	8.57
Antenna Size	m ²	1.3 x 1.3
Element Beamwidth	deg	16.8
Array Beamwidth	mrاد	7.9
Power per Element	dBm	10.0
Number of Elements	-	128
Total Transmit Power	dBm	31.1
Element Noise Figure	dB	5.0
System Noise Bandwidth	GHz	1.0
Number of Frequency Hops	-	5
Pulsewidth	μs	1.0
Noise Equivalent σ ₀ (9000m)	dB	-24.5
Noise Equivalent σ ₀ (500m)	dB	-42.6

The design in Table 1 meets the required parameters through the use of a 0.5m x 0.5m antenna. It contains 128 elements in the array, each transmitting up to 10.0 dBm of power. (It should be noted that this array is highly thinned. This factor helps to save mass and power in the total array. The impact on sidelobes and main beam will not be discussed here, but, given the nadir looking geometry and small scan angles, has been examined and is quite feasible). The element noise figure is assumed to be 8.0 dB. The pulse width must vary as a function of altitude in order to keep the noise equivalent σ₀ above -20 dB, keeping the SNR above -10 dB for even the darkest terrain (for nadir scattering at millimeter waves).

The main difficulty in implementing design 1 is the transmit module power of 10 dBm. This amount of power is high for a simple W-band transmit/receive module, and could require substantial development. This potential challenge has pushed us to a second possible design, a Ka-band system, detailed in Table 3.

The Ka-band system is quite similar in scope to the W-band system, with a 128 element thinned antenna, 10 dBm of power per element (more readily available at Ka-band), a lower system noise figure, and a corresponding lower pulse width. The key difference is the larger antenna of 1.3 m x 1.3 m, which may make accommodation more difficult on the spacecraft.

7. SYSTEM DEVELOPMENT PLANS

We feel that either design discussed in the previous section is viable, and could meet the requirements imposed by the landing and hazard detection systems. Present work includes surveying the available technology to determine which of the two will be developed into a working system prototype over the next two to three years.

In addition to the ongoing frequency / antenna size selection process, we have developed the common radar components, including the ADC, signal generation, and IF receiver portions shown in the Figure 1 block diagram. These components contain the 1 GHz system bandwidth, 5 frequency hops, and 1 Gs/s 2 channel sampling capability required by either of the two designs, and will be used as a future system test bed.

8. SUMMARY

We have developed a millimeter phased array concept that can meet the requirements of a planetary safe landing system. The concept is capable of centimetric accuracy in mean topography, detection of 1m-sized hazards, and measurement of 10cm/s level velocities. We have developed a basic set of key radar parameters, and have begun development of a system prototype.

APPENDIX A

From (4) we see that the argument of the pulse pair product, q , is

$$q = \arg(v_1 v_2^*) = k(r_1 - r_2) = k\Delta r$$

We can write the range difference Δr as

$$\Delta r = (x v_x + y v_y + z v_z) / r$$

If we construct an image of pulse pair products, given the different pointing angles, we can then take partial derivatives across the image as

$$\begin{aligned}\nabla_x q &= s^2 \exp[ik\Delta r] ik \frac{\partial \Delta r}{\partial x} \\ &= q ik \frac{\partial \Delta r}{\partial x} \\ &= q ik v_x / r\end{aligned}$$

We can see that the derivative divided by the original signal is proportional to the velocity. This method can be performed across the image, and the resulting velocities averaged to produce a final product.

ACKNOWLEDGEMENT

This work was performed at the Jet Propulsion Laboratory, California Institute of Technology, under contract with the National Aeronautics and Space Administration (NASA). The authors wish to acknowledge Edward Wong, Andrew Johnson, and Dan Burkhart for their assistance in defining the requirements on the radar for the Mars Science Laboratory mission.

REFERENCES

- [1] E.C. Wong, G. Singh, J.P. Masciarelli, "Autonomous Guidance and Control Design for Hazard Avoidance and Safe Landing on Mars (AIAA-2002-46192)," *Proceedings of the 2002 AIAA Atmospheric Flight Mechanics Conference*, Monterey, CA, August 2002.
- [2] A. Johnson, E.D. Skulsky, M. Bajracharya, and E.C. Wong, "Design of a Hazard Detection and Avoidance System for the Mars Smart Lander (AIAA-2002-4620)," *Proceedings of the 2002 AIAA Atmospheric Flight Mechanics Conference*, Monterey, CA, August 2002.
- [3] C. Elachi, K.E. Im, F. Li, and E. Rodriguez, "Global Digital Topography Mapping with a Synthetic Aperture Scanning Radar Altimeter," *Int. J. Remote Sensing*, vol. 11, no. 4, 585-601, 1990.
- [4] R.J. Doviak and D.S. Zmic, *Doppler Weather Radar Observations*, San Diego: Academic Press, 1993.
- [5] K.S. Miller and M.M. Rochwarger, "A Covariance Approach to Spectral Moment Estimation," *IEEE Trans. on Information Theory*, vol. 18, no. 5, pp 588-596, 1972.

Brian D. Pollard (S'92-M'98) received the Ph.D. in Electrical and Computer Engineering from the University of Massachusetts at Amherst in 1998. His research at the Massachusetts Microwave Remote Sensing Laboratory included the development of a digitally beamformed volume-imaging radar for atmospheric boundary layer (ABL) studies, and compared data from that instrument to large-eddy simulations of the ABL. Dr. Pollard joined the Jet Propulsion Laboratory in 1998, where his research interests include high precision altimetry and

interferometry for oceanic, terrestrial, and planetary applications.

Delwyn Moller received a Bachelor of Engineering degree (1990) and a Master of Engineering degree (1992) from the University of Auckland, New Zealand. In 1997 she then completed a Ph.D. in radar remote sensing at the University of Massachusetts. She joined the Jet Propulsion Laboratory in 1997 where she is a Member of Technical Staff in the Radar Science and Engineering Section. Her tasks in this position have included system engineering and performance evaluation on a number of projects including the Shuttle Radar Topography Mission (SRTM), data-acquisition system design, and data analysis and processing for along-track interferometry.

Ernesto Rodriguez joined the Jet Propulsion Laboratory in 1985. He is currently supervisor of the Interferometric Synthetic Aperture Radar Phenomenology group.